Development of an Underwater Manipulator and Its Free-Floating Autonomous Operation

Yu Wang, Shuo Wang, Qingping Wei, Min Tan, Chao Zhou, and Junzhi Yu, *Senior Member, IEEE*

***Abstract*—This paper addresses the novel design of an underwater manipulator with a lightweight multilink structure and its free-floating autonomous operation. The concept design reduces the coupling between the manipulator and the vehicle efficiently, even in the case where the vehicle weight in air is not significantly greater than the manipulator weight. The specific implementation of the mechanical structure is elaborated. Moreover, a closed-loop control system based on binocular vision is proposed for underwater manipulation. In the end, experimental results demonstrate that the conceived underwater manipulator can accomplish the autonomous operation quickly.**

***Index Terms*—Autonomous operation, free-floating manipulation, underwater manipulator, UVMS.**

I. Introduction

RECENTLY, the development of offshore engineering has drawn extensive attention. Different types of underwater vehicles have been developed for applications [1]–[5]. However, most underwater assigned tasks are still accomplished under the supervision and remote control of human beings. Therefore, it becomes a trend that an underwater vehicle-manipulator system (UVMS) achieves complicated and specific tasks (such as rescue, salvage, collection) autonomously, instead of human beings. Autonomous manipulation is a challenging control problem, because an UVMS belongs to a nonlinear, highly redundant, and high-dimensional system [6]. Generally, the vehicle thrusters are applied to compensate for the arm's reaction, but sometimes it is not effective due to the difficulty of hovering control of the vehicle [7]. Therefore, a simple and direct method is easily considered to reduce the motion of the UVMS caused by the arm's movement, this is to let the vehicle be far larger than the manipulator. This vehicle with large size can be applied in spacious environments, but is not practical in relatively narrow space. Hence, we design a novel mechanical structure of an underwater manipulator which can reduce the coupling between the manipulator and the vehicle drastically. Furthermore, this manipulator can be applied to perform autonomous manipulation in a short time.

Remarkably, many companies have developed various types of underwater arms. In [8], the specific performance parameters of different types of underwater arms have been summarized. As Fernandez *et al.*, described, these underwater manipulators are generally used for remote operation because of large mass and volume. Once the vehicle is equipped with one of these manipulators, it needs to overcome the large reaction of the manipulator.

Therefore, some researchers have studied kinematics and dynamics modeling of UVMSs for motion control. Antonelli gave the kinematics of UVMSs [9]. Tarn *et al.*, adopted Kanes method to accomplish the dynamics modeling of an underwater vehicle with a manipulator [10]. Korkmaz *et al.*, modeled the dynamics of an UVMS considering hydrostatic forces and hydrodynamic effects [11]. Han *et al.*, presented a framework for actively using the restoring moments of an UVMS based on kinematics and dynamics modeling of an UVMS [12], [13]. Analogously, Santhakumar detailed the kinematics and dynamics modeling of an UVMS considering the coupling between the vehicle and the manipulator [14]. Additionally, there have been many control methods to realize the vehicle-arm coordination for the purpose of autonomous manipulation considering its coupling. Lynch and Ellery used the methods including feedback and feedforward control to achieve the coordination control of an UVMS [15]. Sarkar and Podder proposed a motion coordination algorithm for an UVMS, which minimized the total drag on the system by utilizing the null-space vector based on the gradient projection optimization technique [16]. Mohan and Kim developed an indirect adaptive control scheme based on an improved Kalman filter to perform underwater execution [17]. Santhakumar presented a task-space control method for an UVMS to accomplish underwater intervention [18]. Besides, hybrid control with fuzzy controller has been utilized for the coordination control. Antonelli and Chiaverini combined a task-priority inverse kinematics approach and a fuzzy method to perform motion coordination of an UVMS, and the fuzzy method was employed to distribute the motion between the vehicle and the manipulator [19], [20]. Analogously, Farias dos Santos and de Pieri applied hybrid control, which was a combination of a functional machine and fuzzy approach, to complete the vehicle-arm coordination [21]. And Xu *et al.*, proposed a neuro-fuzzy controller to realize the tracking control of the UVMS as well [22]. Furthermore, autonomous control of an UVMS with multiple control objectives has been investigated. Olguin-Diaz *et al.*, presented a

Manuscript received November 3, 2014; revised July 12, 2015; accepted September 23, 2015. Date of publication October 26, 2015; date of current version February 24, 2016. Recommended by Technical Editor O. Kaynak. This work was supported in part by the National Natural Science Foundation of China under Grant 51175496, Grant 61333016, Grant 61273337, and Grant 61473295, in part by the Foundation for Innovative Research Groups of the National Natural Science Foundation of China under Grant 61421004, and in part by the Beijing Natural Science Foundation under Grant 3141002.

The authors are with the State Key Laboratory of Management and Control for Complex Systems, Institute of Automation, Chinese Academy of Sciences, Beijing 100190, China (e-mail: yu.wang@ia.ac.cn; shuo.wang@ia.ac.cn; qingping.wei@ia.ac.cn; min.tan@ia.ac.cn; chao.zhou@ia.ac.cn; junzhi.yu@ia.ac.cn).

Color versions of one or more of the figures in this paper are available online at http://ieeexplore.ieee.org.

Digital Object Identifier 10.1109/TMECH.2015.2494068

passivity-based force-motion control scheme, which could concurrently track the end-effector pose, operational force, and posture references [23]. Beside, Ismail and Dunnigan proposed a tracking control scheme which could not only track the prescribed subregion but also perform various subtasks [24]. But unfortunately, the above methods have not been applied in the actual systems.

In fact, only a few UVMSs for autonomous manipulation have been developed according to the authors' knowledge. Sakagami *et al.*, provided an attitude control system for the developed underwater robotic system with manipulators [25]. However, there is no report about autonomous intervention. The contributions of the following two projects must be worth mentioning. In the SAUVIM project, a semi-autonomous underwater vehicle with a 7 degrees of freedom (DoF) arm for intervention mission was developed, and autonomous intervention was performed [26], [27]. In the TRIDENT project, an AUV named GIRONA 500 was specially designed for autonomous manipulation. It could be equipped with a lightweight ARM 5E manipulator or a Graal Tech manipulator. Floating underwater manipulation was successfully achieved [8], [28]–[33]. Nevertheless, high arm velocities would lead to the amplified dynamic coupling between the manipulator and the vehicle [8].

The main contribution of this paper is the design of a new underwater manipulator with a lightweight multilink structure, which can be assembled on an autonomous underwater vehicle. This concept design can reduce the coupling between the manipulator and the vehicle efficiently, even in the case where the vehicle weight in air is not significantly greater than the manipulator weight. Moreover, a closed-loop control system based on binocular vision is proposed for grasping. Finally, the underwater manipulator is attached to our floating robot "Robocutt-I," in the head of which, two cameras have been installed. The autonomous underwater manipulation can be implemented quickly. In our experiment, the average execution time is about 2.96 s.

The rest of the paper is arranged as follows. The concept design and kinematics analysis of the underwater manipulator are presented in Section II, where its mechanical design is detailed. The closed-loop control system based on vision is proposed for autonomous manipulation in Section III. Experiments and discussions are given in Section IV and Section V, respectively. Finally, conclusion and future work are summarized in Section VI.

II. Concept Design and Kinematics Analysis

The main objective of the proposed underwater manipulator is to realize the autonomous operation for underwater robots. The underwater autonomous manipulation of an UVMS is a challenging and very heated topic because of the coupling between the manipulator and the vehicle. The impact on the movement of the vehicle related to the volume ratio and weight ratio between the manipulator and the vehicle has been quantitatively discussed [34], [35]. Furthermore, it has been summarized that the lower the volume ratio and weight ratio between the manipulator and the vehicle, the more stable the vehicle will be. As a consequence, we design a novel underwater manipulator with a lightweight multilink structure to reduce the volume ratio and weight ratio between the manipulator and the vehicle efficiently.

A. Mechanical Design

Usually, the motors are mounted near the driven joints in the traditional underwater manipulator. This mechanical structure results in large mass of the manipulator. Hence, the volume of the manipulator can be increased in order to reduce the dynamic coupling between the manipulator and the vehicle. For example, the designed underwater manipulator in [8] was covered with foam material to guarantee sufficient sustenance for light weight in water. However, because of its big volume, added mass and resistance are increased to still amplify the coupling between the manipulator and the vehicle. Compared with the traditional underwater manipulators, the novel underwater manipulator with a waterproof base and a lightweight multilink structure is developed. On one hand, all the servo motors which drive the multilink structure and their controllers are integrated inside the waterproof base. On the other hand, the lightweight multilink structure is served as a manipulation tool. The connections between servo motors and the joints of the lightweight multilink structure are achieved by timing belt pulley, gear, or wire rope transmission. This design leads to a good performance: the base weight in air is 11.04 kg, while the mass of the multilink structure is 0.889 kg. Thus, the center of the manipulator's gravity is located in the base unit. As the waterproof base unit is attached to the vehicle, the movement of the multilink structure has small impact on the pose of the UVMS.

The description of this new mechanical design is shown in Fig. 1. It is a 5 DoF manipulator, which is composed of a waterproof base, a multilink structure, Waist joint, and Gripper. The four servo motors and their controllers are placed inside the waterproof base. Two rods and the Gripper with small volume and light weight constitute the multilink structure, which is regarded as the manipulation tool. Additionally, the Waist joint installed in the interior of the vehicle is added to rotate the waterproof base. This novel structure greatly lowers the coupling between the manipulator and the vehicle, which provides the foundation for a relative high-speed underwater operation.

As depicted in Fig. 2, the initial position of the manipulator is defined: Link 1 and 2 are both parallel to the horizontal plane. The plane formed by the open Gripper is also parallel to the horizontal plane. Moreover, Gripper is closed. So the Denavit–Hartenberg (D–H) reference frames including $O_0X_0Y_0Z_0 \sim O_4X_4Y_4Z_4$ are assigned. a_1 is the link length between Waist and Shoulder, a_2 is the link length between Shoulder and Elbow, d_4 is the offset. $\theta_1, \theta_2, \theta_3, \theta_4$ represent the joint angles of Waist, Shoulder, Elbow, and Wrist, respectively. $\theta_i (i = 1, 2, 3, 4)$ is defined as the rotational angle around the corresponding joint axis, which is also Z_{i-1} axis. θ_5 is defined as the opening angle of Gripper. All the joint angles are 0° when the manipulator is in the initial position as illustrated in Fig. 2. In practice, the initial position of the manipulator is determined by optoelectronic switches. Next, we detail the specific implementation of the mechanical structure.

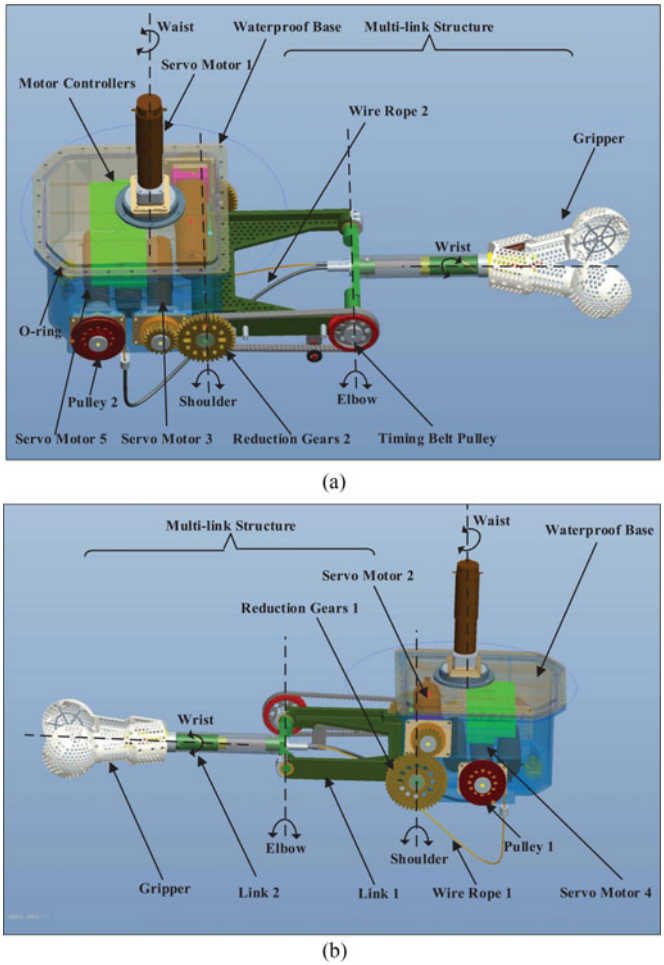

Fig. 1. Mechanism design of the manipulator. (a) Right view of the manipulator. (b) Left view of the manipulator.

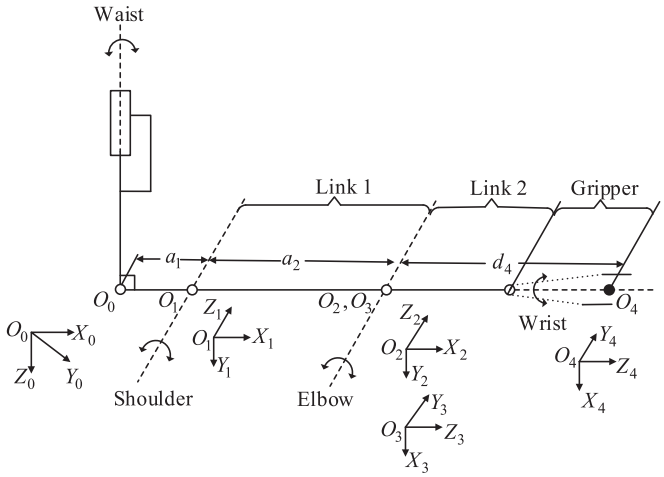

Fig. 2. D–H reference frames.

1) Implementation of Shoulder and Elbow: As shown in Fig. 1, the Shoulder joint is actuated by Servo Motor 2, and the transmission is Reduction Gears 1 including a large-diameter portion and a small-diameter portion. The large-diameter one is connected to the shaft of Shoulder. The other one is connected to the shaft of Servo Motor 2. In addition, the Elbow joint is actuated by Servo Motor 3, and the transmissions are Reduction Gears 2 and Timing Belt Pulley. The large-diameter portion of Timing Belt Pulley is connected to the shaft of Elbow. The small-diameter portion of Reduction Gears 2 is connected to the shaft of Servo Motor 3. All the above connections belong to the rotationally fixed manner by keys. But the small-diameter portion of Timing Belt Pulley and the large-diameter portion of Reduction Gears 2 are fixed together by a key to form an unit. This integrated unit is connected to the shaft of Shoulder by a bearing. Owing to this implementation, Elbow joint angle is influenced by not only the rotational angle of Servo Motor 2, but also the rotational angle of Servo Motor 3. The Shoulder joint angle θ_2 and Elbow joint angle θ_3 are determined by

$$\theta_2 = n_1 \cdot \theta_{\text{Motor2}} \tag{1}$$

$$\theta_3 = n_1 \cdot n_3 \cdot \theta_{\text{Motor2}} + n_2 \cdot n_3 \cdot \theta_{\text{Motor3}} \tag{2}$$

where θ_{Motor2} and θ_{Motor3} represent the rotational angle of Servo Motor 2 and Servo Motor 3, respectively, n_1, n_2, n_3 represent the reduction ratios of Gears 1, Gears 2, and Timing Belt Pulley, respectively.

2) Implementation of Wrist and Gripper: As illustrated in Fig. 1, the Wrist joint is actuated by Servo Motor 4, and the transmission is Wire Rope 1. Fig. 3 further details the implementation from State 1 to 2. State 1 represents the status of the arm, where Wrist is in its initial position($\theta_4 = 0$) and Gripper is closed, while State 2 represents the status of the arm, where Wrist is rotated to an angle ($\theta_4 \neq 0$) and Gripper is open with the angle of θ_5 ($\theta_5 \neq 0$). As depicted in Fig. 3, Wire Rope 1 is fixed to draw-bar 1 by a screw, Pin 1 is fixed into draw-bar 1, and a helix trajectory is inserted into the stick which is fixed to Gripper. The projection of this helix trajectory on the x_d–y_d plane is a circle with a radius of r. The helix curve equation in the assigned reference frame $o_d x_d y_d z_d$ is expressed by

$$\begin{cases} x^2 + y^2 = r^2 \\ \dfrac{z}{L} = \dfrac{\theta_4}{2\pi} \end{cases} \tag{3}$$

where L is the distance between the initial point and the end point of the helix curve along z_d-axis as marked in Fig. 3. Note that the stick is fixed to Gripper and they can be rotated together. Moreover, draw-bar 1 can only do the linear motion repeatedly. Hence, Pin 1 will move along a straight line to push the stick and Gripper to rotate together if Wire Rope 1 drags draw-bar 1. Beside, as the movement of draw-bar 1 makes Spring 1 compressed, Spring 1 could push draw-bar 1 to make Gripper rotated reversely in case of the backward rotation of Servo Motor 4. Thus, Servo Motor 4 can actuate Wrist by Wire Rope 1. The relationship between θ_4 and the rotational angle of Servo Motor 4 (denoted by θ_{Motor4}) can be obtained as

$$\theta_4 = \frac{2\pi R_1 \theta_{\text{Motor4}}}{L} \tag{4}$$

where R_1 denotes the radius of Pulley 1 winded by Wire Rope 1. Pulley 1 is connected to the shaft of Servo Motor 4 by a key [See Fig. 1(b)].

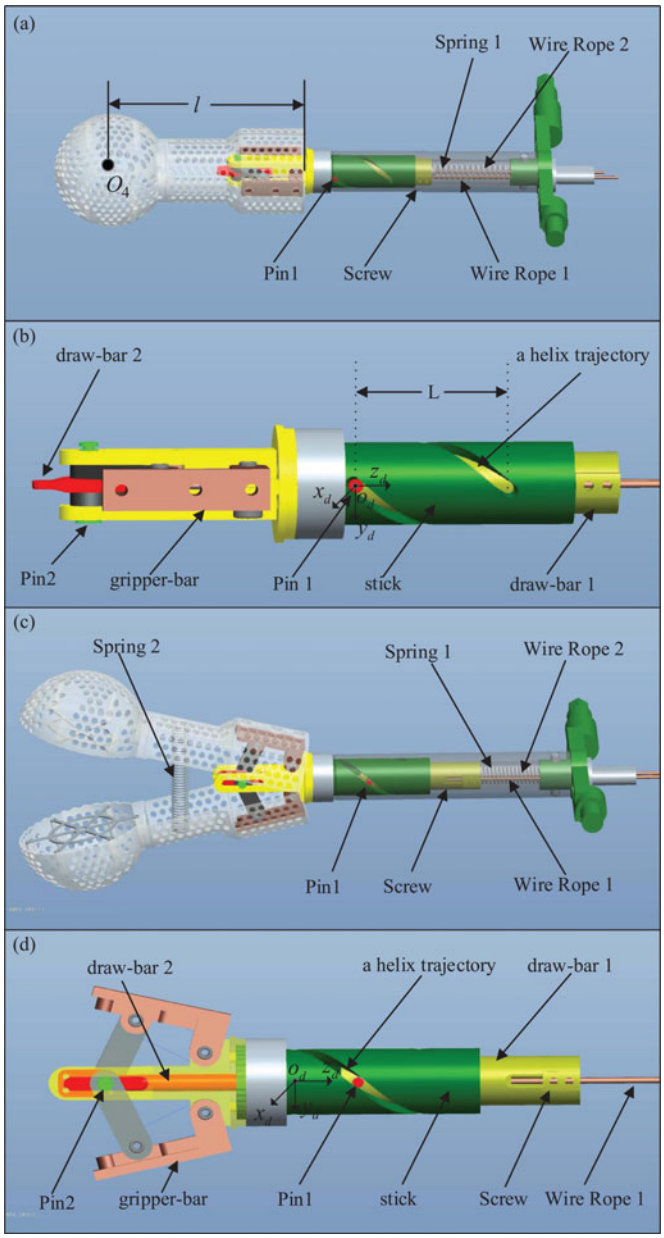

Fig. 3. Implementation of Wrist and Gripper from State 1 rto State 2. (a) State 1. (b) Specific implementation of Wrist and Gripper in State 1. (c) State 2. (d) Specific implementation of Wrist and Gripper in State 2.

Analogously, Gripper is actuated by Servo Motor 5, and the transmission is Wire Rope 2. Wire Rope 2 is fastened to draw-bar 2 by a binding screw. Pin 2 is fixed into draw-bar 2. Pin 2 will move and Gripper is open if Wire Rope 2 drags draw-bar 2. There is a pullback spring mounted in Gripper to make Gripper closed, when Servo Motor 5 is rotated in the opposite direction. As demonstrated in Fig. 4, the realization of the action from closed Gripper to open Gripper is given. Since several mechanical parameters including $l_1 \sim l_4$ (as marked in Fig. 4) are invariable and θ_g (as marked in Fig. 4) is variable, the opening action and closing action of Gripper can be implemented by the translation of Pin 2. Therefore, we can get

$$(l_4 - l_2\cos\theta_g - l_g)^2 + (l_2\sin\theta_g + l_3)^2 = l_1^2 \tag{5}$$

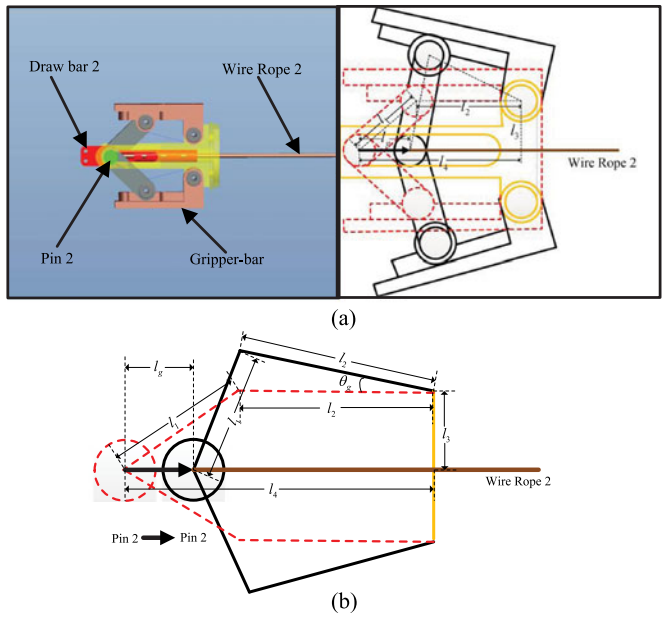

Fig. 4. Implementation of Gripper. (a) Mechanical structure of Gripper. (b) Simplified schematic diagram for the realization of the action from closed Gripper to open Gripper.

where l_g represents the translation distance of Pin 2, l_1–l_4 represent several fixed mechanical lengths. It is noted that l_1–l_4 constitute a right-angled trapezoid when Gripper is closed. Pulley 2 is connected to the shaft of Servo Motor 5 by a key see Fig. 1(a)]. R_2 denotes the radius of Pulley 2 winded by Wire Rope 2, θ_5 and θ_{Motor5} denote the opening angle of Gripper and the rotational angle of Servo Motor 5, respectively. By substituting $l_g = R_2 \cdot \theta_{\text{Motor5}}$, $\theta_g = \frac{1}{2}\theta_5$ into (5), we can obtain the relationship between θ_5 and θ_{Motor5}:

$$A \cdot \cos\frac{1}{2}\theta_5 + B \cdot \sin\frac{1}{2}\theta_5 = C \tag{6}$$

where A, B, C are calculated as

$$\begin{aligned} A &= 2l_2R_2\theta_{\text{Motor5}} - 2l_2l_4 \\ B &= 2l_2l_3 \\ C &= l_1^2 - l_4^2 - R_2^2\theta_{\text{Motor5}}^2 - l_2^2 - l_3^2 + 2l_4R_2\theta_{\text{Motor5}}. \end{aligned} \tag{7}$$

3) Implementation of Waist: Taking account of expanding the manipulator's workspace, the Waist joint is added. The waterproof base is mounted on the bottom of the underwater vehicle. The Waist joint is actuated by Servo Motor 1 (see Fig. 1), and Servo Motor 1 is fixed in the interior of the vehicle. In order to further reduce the coupling of the UVMS, the centers of the manipulator's mass and buoyancy are set on the same vertical line, when the manipulator is in the predefined initial position. This vertical line coincides with the rotation axis of Waist. The setting for the centers of the manipulator's mass and buoyancy can be achieved by changing the positions of servo motors in the base unit during the design. The employment of this setting can reduce the impact induced by the motion of Waist. Namely, this arrange guarantees small changes of the centers of

TABLE I
MAIN COMPONENTS' WEIGHT

Components	Weight in air(kg)	Weight in water(kg)
Base unit	11.04	4.39
Link 1	0.44	0.159
Link 2	0.311	0.106
Gripper	0.138	0.043
Total structure	11.929	4.698

TABLE II
MECHANICAL PARAMETERS OF THE UNDERWATER MANIPULATOR

Parameters	Value	Parameters	Value
l_1	25 mm	R_1	35mm
l_2	24 mm	R_2	35mm
l_3	15 mm	n_1	20/44
l_4	44 mm	n_2	20/37
L	40 mm	n_3	32/40

the manipulator's mass and buoyancy, once the waterproof base is rotated.

Based on the aforementioned mechanical design, an underwater manipulator has been developed. Table I tabulates the weight of the main components of the underwater manipulator, and Table II tabulates the values of the mechanical parameters as mentioned above. The base unit occupies a considerable proportion of the weight of the underwater manipulator: the base weight in air is 11.04 kg, while the mass of the multilink structure is 0.889 kg. Benefiting from this mechanical design, the coupling between the manipulator and the vehicle is reduced significantly. Thus, the relative high-speed underwater operation could become feasible.

B. Kinematics and Inverse Kinematics of the Manipulator

Since Denavit–Hartenberg (D–H) reference frames are given in Fig. 2, the kinematics of the underwater manipulator is easy to be established based on the D–H parameters model. Hence, the position and orientation of the end effector in the $O_0X_0Y_0Z_0$ frame are obtained by

$$
\begin{aligned}
{}^0T_E &= \begin{bmatrix} {}^0R_E & {}^0P_E \\ 0 & 1 \end{bmatrix} \\
&= A_1(\theta_1, a_1) \cdot A_2(\theta_2, a_2) \cdot A_3(\theta_3) \cdot A_4(\theta_4, d_4) \quad (8)
\end{aligned}
$$

where ${}^0R_E = [N_E, O_E, A_E]$ and ${}^0P_E = [p_x, p_y, p_z]^T$ are the orientation matrix and the position vector of the end effector in the $O_0X_0Y_0Z_0$ frame, respectively; A_1, A_2, A_3 and A_4 are the transformation matrices of the link frames. Here, $N_E = [n_x, n_y, n_z]^T$, $O_E = [o_x, o_y, o_z]^T$, $A_E = [a_x, a_y, a_z]^T$. The specific D–H parameters are listed in Table III. Therefore,

TABLE III
D–H PARAMETERS

Link	$\theta(^\circ)$	d(mm)	a(mm)	$\alpha(^\circ)$
1	θ_1	0	67	90
2	θ_2	0	189.95	0
3	$\theta_3 + 90$	0	0	90
4	θ_4	323	0	0

we can get the forward kinematic equations

$$
\begin{cases}
p_x = \cos\theta_1(d_4\cos(\theta_2+\theta_3) + a_1 + a_2\cos\theta_2) \\
p_y = \sin\theta_1(d_4\cos(\theta_2+\theta_3) + a_1 + a_2\cos\theta_2) \\
p_z = a_2\sin\theta_2 + d_4\sin(\theta_2+\theta_3)
\end{cases} \quad (9)
$$

By the derivation of (9), we can get

$$
p_z\sin\theta_2 + D\cos\theta_2 = E \quad (10)
$$

where

$$
\begin{aligned}
D &= \sqrt{p_x^2 + p_y^2} - a_1 \\
E &= \frac{\left(\sqrt{p_x^2 + p_y^2} - a_1\right)^2 + a_2^2 + p_z^2 - d_4^2}{2a_2} \quad (11)
\end{aligned}
$$

Considering the cameras' field of view, θ_1, θ_2, and θ_3 should be limited in the corresponding ranges:

$$
\begin{cases}
\theta_1 \in (-30^\circ, 30^\circ) \\
\theta_2 \in (0, 90^\circ) \\
\theta_3 \in (-150^\circ, 0^\circ)
\end{cases} . \quad (12)
$$

Therefore, θ_2 can be determined by (10) and (12). Then θ_1 and θ_3 are computed by substituting θ_2 into (9). According to (8), we can get

$$
{}^0T_E \cdot A_4^{-1} = A_1 \cdot A_2 \cdot A_3 = \ell_{4\times4} \quad (13)
$$

where, $\ell_{4\times4}$ is a 4×4 matrix related to the parameters θ_1, θ_2, θ_3, a_1, a_2. This matrix is known. Moreover, Equation (14) as shown at the bottom of the next page. Therefore, θ_4 could be calculated by (13) and (14).

III. DESIGN OF THE VISION-BASED CONTROL SYSTEM

A. System Configuration

By the special schedule of mechanical structure, a newly designed manipulator with a lightweight multilink structure has been developed. In order to illustrate the rationality of the mechanical structure, this manipulator is installed on a vehicle for free-floating underwater manipulation as seen in Fig. 5(a). The Waist joint of the manipulator is integrated inside the vehicle. The vehicle is composed of a cylinder and two hemispherical cavities with a diameter of 260 mm. The cylinder's bottom diameter is 260 mm and height is 550 mm. The vehicle weight in air is 27 kg, and the weight of water displaced by the vehicle

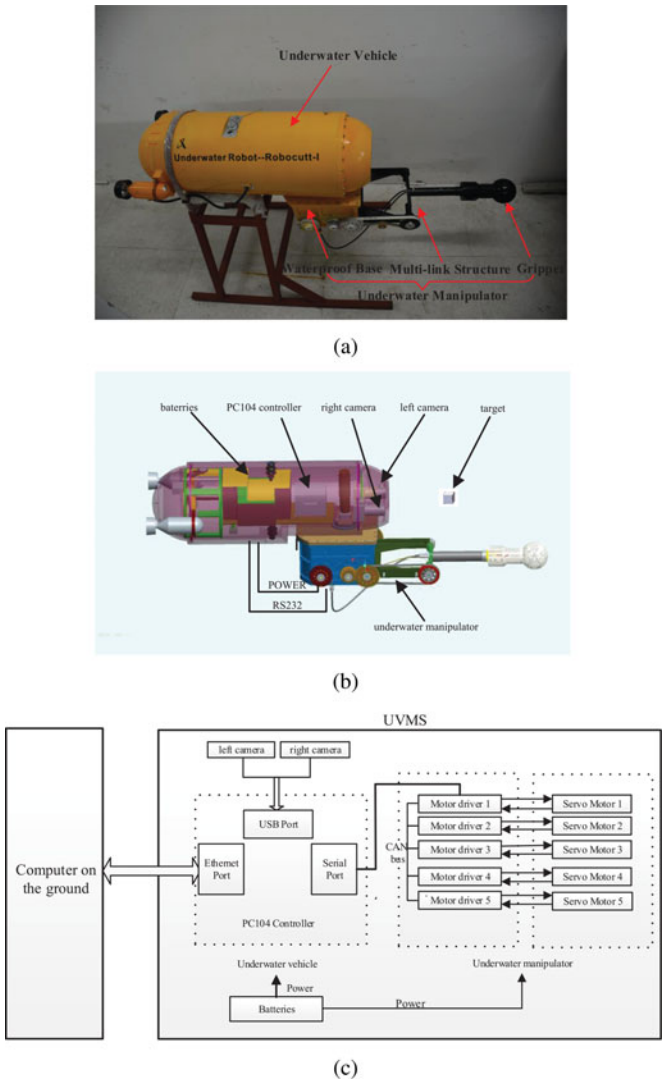

Fig. 5. Configuration of the UVMS. (a) Robotic prototype. (b) Concept design. (c) System hardware configuration.

completely submerged into water is 31.698 kg. As the manipulator weight in water is 4.698 kg (See Table I), the UVMS could just be suspended in water. The comprehensive overview of the system configuration is introduced as seen in Fig. 5(b) and (c). This system is composed of batteries, the underwater manipulator with a multilink structure, a vision system with two cameras and a $PC104$ controller. Batteries, which provide the power for the manipulator and the $PC104$ controller, are mounted inside the underwater vehicle. The underwater manipulator is implemented as primitively described. The vision system is installed in front of the underwater vehicle. The image captured by the respective camera is processed to recognize the target. The target position in the $O_0X_0Y_0Z_0$ frame (marked in Fig. 2) is calculated and served as the given input of the control system. In addition, the vision-based control system is achieved by the $PC104$ controller.

B. Control System Design

The diagram of the vision-based control system is depicted in Fig. 6. This control system consists of image processing, position filtering, inverse kinematics, angle conversion, and servo motion control. The vision system with two cameras is applied to measure the target position as the input of the control system. The pose of the UVMS is changing due to the coupling of the manipulator and the vehicle during arm maneuvers. Consequently, the target position in the $O_0X_0Y_0Z_0$ frame needs to be updated ceaselessly. Image processing is used to achieve target recognition and calculate the target position. Position filtering is employed to improve the precision of the target position computed by the visual system. Angle conversion realizes the conversion from θ_i to θ_{Motori} $(i = 1, 2, 3, 4, 5)$, which is obtained by the relationship between θ_i and θ_{Motori}. This relationship and inverse kinematics of the underwater manipulator are described in Section II-A and II-B, respectively. Since the joint positions of the underwater manipulator need high speed and the accuracy of absolute position, two closed loops of the motor including velocity loop and position loop are applied to realize the control of dc servo motor. These two closed loops are marked in Fig. 6. Their feedback signals are both from the difference of the optical encoder data. The detailed description of servo motor control has been given in [36]. Thus, it is omitted. Next, image processing are detailed.

1) Image Processing: The vision system is used once the positions of the target center in the images captured by the two cameras are available. And the target position in the $O_0X_0Y_0Z_0$ frame could naturally be computed by 3-D reconstruction method. So, we briefly describe the determination of the position of the target center in the image as illustrated in Algorithm 1, where T_{area} is defined as the threshold value of the region of interest (ROI).

For simplicity, the object with red-color feature is selected as the target. Therefore, the threshold segmentation is applied to obtain the target area which is defined as

$$\begin{aligned} S &= S_1 \cap S_2 \\ S_1 &= ((i,j) \mid P^R_{i,j} > T_1, P^R_{i,j} > k_{rg} P^G_{i,j}, P^R_{i,j} > k_{rb} P^B_{i,j}) \\ S_2 &= ((i,j) \mid P^R_{i,j} - P^G_{i,j} > T_2, P^R_{i,j} - P^G_{i,j} > T_3) \end{aligned} \tag{15}$$

$$ {}^0T_E A_4^{-1} = \begin{bmatrix} n_x \cos\theta_4 - o_x \sin\theta_4 & o_x \cos\theta_4 + n_x \sin\theta_4 & a_x & p_x - a_x d_4 \\ n_y \cos\theta_4 - o_y \sin\theta_4 & o_y \cos\theta_4 + n_y \sin\theta_4 & a_y & p_y - a_y d_4 \\ n_z \cos\theta_4 - o_z \sin\theta_4 & o_z \cos\theta_4 + n_z \sin\theta_4 & a_z & p_z - a_z d_4 \\ 0 & 0 & 0 & 1 \end{bmatrix}. \tag{14}$$

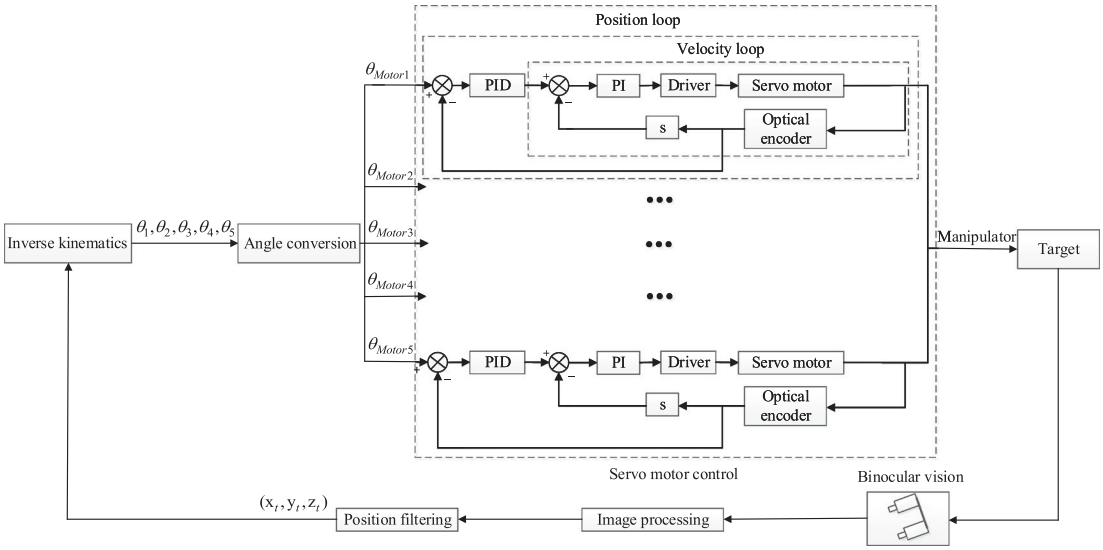

Fig. 6. Block diagram of the vision-based control system.

Algorithm 1 the determination of the position of the target center

```
while (1) do
    Image capture.
    get the ROI based on image segmentation.
    if (the ROI is smaller than T_area) then
        Break.
    else
        Canny edge detection algorithm for the ROI image.
        get the binary image.
        extract all the contours in the binary image.
        compute the area of every contour.
        find the contour with the maximum area as the
        target contour.
        compute the center of the target contour.
    end if
end while
```

where $P_{i,j}^R$, $P_{i,j}^G$, and $P_{i,j}^B$ are the values of R, G, B components of pixel point (i, j), respectively, k_{rg} is the threshold value of the ratio of R component to G component, k_{rb} is the threshold value of the ratio of R component to B component, T_1, T_2, T_3 are the threshold values.

In order to get the target position in the $O_0X_0Y_0Z_0$ frame, the target center in the images of the two cameras should be determined. Because some pixels with similar color feature in the image may mistakenly belong to the target, all the contours in the image firstly should be extracted in the binary image, and the contour with the largest area is chosen as the target. The center of all contour pixels is served as the position of the target center in the image. Hence, the position of the target center in the $O_0X_0Y_0Z_0$ frame is obtained using vision positioning system. Fig. 7 shows the determination of the underwater target in the images captured by the two cameras, respectively. Thus, the position of the target center in the $O_0X_0Y_0Z_0$ frame can be obtained by 3-D reconstruction method, which could be found in [37]. Note that the parameters of the cameras need to be calibrated in water.

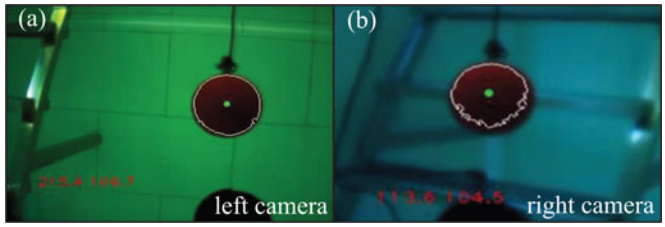

Fig. 7. Image Processing. (a) Left camera. (b) Right camera.

IV. Experiment and Results

In order to illustrate the rationality of the mechanical structure, the experiment of free-floating autonomous manipulation is performed in a water pool. The detailed experiment system is described in Fig. 5. The system processer is a 1.8 -GHz Pentium-class PC104 controller with 1-Gb RAM, and there are two cameras in front of the vehicle. The calibration of the intrinsic parameters and external parameters of the vision system and hand-eye calibration have been prematurely completed in water.

In the experiment, we just conduct autonomous manipulation but not consider the motion of the UVMS. Hence, a red target tied by a rope is placed in the vision system, then the position of the target is computed, and free-floating autonomous manipulation is realized. We randomly place the target at different initial positions which are in the view of binocular system, then the autonomous execution starts off. Fig. 8 shows the relationship between the execution time and the distance between the initial position of target and the initial position of Gripper. The average execution time spent on the processes of approaching the target and closing the Gripper is 2.96 s.

The autonomous operation is deduced when the initial position of target in the $O_0X_0Y_0Z_0$ frame is $(470.23, -26.25,$

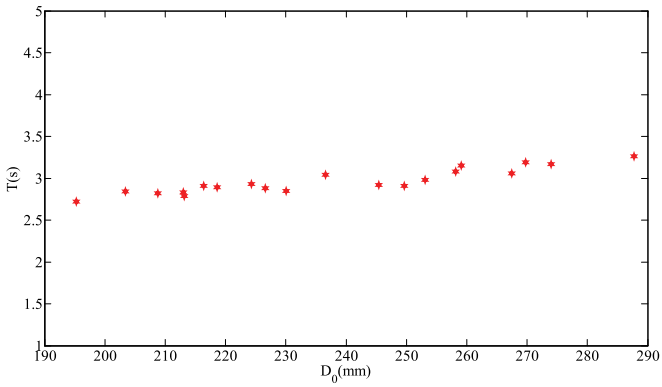

Fig. 8. Execution time versus the distance between the initial position of target and the initial position of Gripper. The execution time is denoted by T, and the distance between the initial position of target and the initial position of Gripper is denoted by D_0.

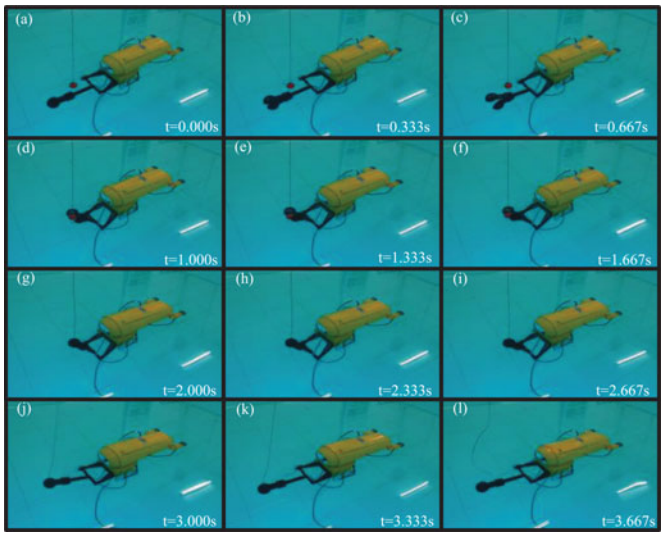

Fig. 9. Consecutive snapshots of free-floating autonomous manipulation.

-175.63). Consecutive snapshots of free-floating autonomous manipulation are given in Fig. 9, where Fig. 9(a)–(f) show the process of approaching the target, Fig. 9(g)–(i) show the process of closing the Gripper, and Fig. 9(j)–(l) show the process of returning to the initial position. The graph reflecting time history of the positions of target and end-effector in the $O_0X_0Y_0Z_0$ frame is depicted in Fig. 10, where D is defined as the distance between the target and end-effector. The X value of the target in the $O_0X_0Y_0Z_0$ frame is progressively smaller see Fig. 10(a)], which illustrates that forward movement of the vehicle with respect to the target is produced during arm maneuvers. Additionally, from the change rules of the Z value of the target, it can be seen that the head of the UVMS is pitched up during manipulator maneuvers, and then the head returns to the original angle after the approaching process is over [see Fig. 10(c)].

Autonomous manipulation has made a great progress in FP7-TRIDENT project [8], [28]–[30]. Similarly, autonomous operation for the object whose weight is less than 1.5 Kg could be accomplished in our platform. The motion control of the vehicle

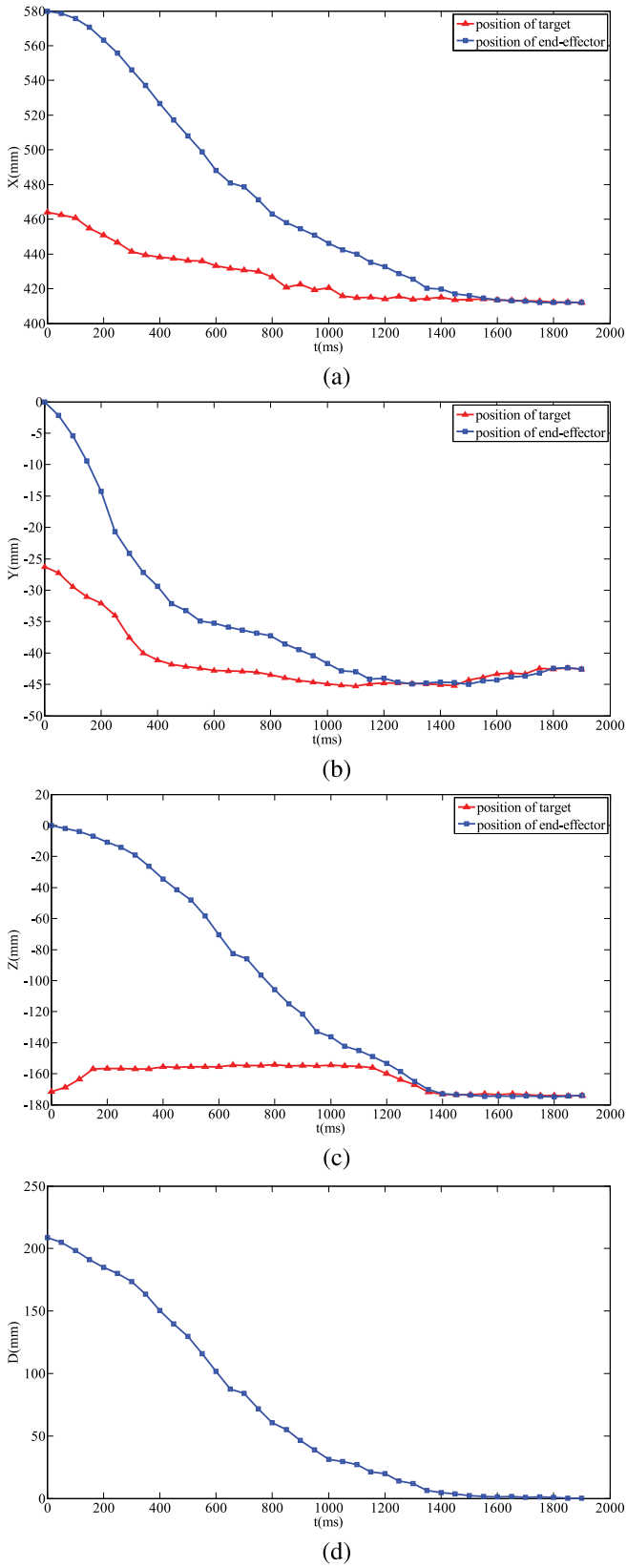

Fig. 10. Time history of positions of the target and end-effector in the reference $O_0X_0Y_0Z_0$ frame. (a) Time history of X values of the target and end-effector. (b) Time history of Y values of the target and end-effector. (c) Time history of Z values of the target and end-effector. (d) Time history of D, which is defined as the distance between the manipulator end effector and the target.

has been taken into account in [8], which is not considered in our current study. The average time spent on the processes of approaching the target and closing the Gripper using the developed manipulator is about 2.96 s. Overall, the experiment demonstrates that the novel mechanical design reduces the coupling between the manipulator and the vehicle drastically. Owing to this, free-floating autonomous manipulation can be achieved in a short time.

V. Discussion

Increased attention has been given to underwater operation of the UVMS. However, most platforms are remotely controlled by human beings, and just a few ones can achieve autonomous manipulation. Moreover, the impact caused by the motion of the manipulator usually needs to be restrained by coordination control between the vehicle and the manipulator [8]. Hence, we attempt to design a novel mechanism to reduce this dynamic coupling caused by the motion of the manipulator and achieve autonomous manipulation at a relative high speed. Zhang *et al.* [34] and Barbalata *et al.* [35] gave the quantitative discussion about the impact on the movement of the vehicle related to volume ratio and weight ratio between the manipulator and the vehicle. The main superiority of the developed manipulator is that the volume ratio and weight ratio between the manipulator and the vehicle are markedly reduced, which leads to small impact on the vehicle movement. We provide experimental results to prove that the novel design leads to small dynamic coupling between the manipulator and the vehicle, even in the case where the vehicle weight in air is not significantly greater than the manipulator weight. Meanwhile, autonomous execution is achieved in a short time. However, wire rope transmission is used to implement the connections between servo motors and the joints. The deformation of wire ropes will exist after the long-term use of the manipulator. So the initial position of the manipulator needs to be calibrated termly to guarantee its working precision. Moreover, we lay stress on the realization of autonomous manipulation, but just a target with special features is recognized in image processing.

The main emphasis places on the novel mechanism of the manipulator and its free-floating autonomous operation in this paper. In the experiment, we place the target within the manipulator's workspace. Because the changes of the UVMS position are small when the arm is moving, the target is still in the grab range of the UVMS. Thus, autonomous manipulation can be achieved. Note that the object weight should be less than 1.5 Kg. The coordination control between the manipulator and the vehicle is not considered.

VI. Conclusion and Future Work

The development of a novel underwater manipulator has been presented, and its free-floating autonomous operation has been achieved. In the design of mechanical structure, motors and controllers are placed inside the waterproof base, which is installed on the vehicle. The waterproof base occupies most of the underwater manipulator's mass. This concept design reduces the dynamic coupling between the manipulator and the vehicle significantly. In order to realize free-floating autonomous operation, the vision-based control system is proposed. Physical experiments are conducted to verify that this manipulator can achieve free-floating autonomous operation in a short time.

Future research will concentrate on the vehicle-arm coordination control.

References

[1] J. H. Kim, J. C. Lee, and Y. R. Choi, "LAROB: Laser-guided underwater mobile robot for reactor vessel inspection," *IEEE/ASME Trans. Mechatron.*, vol. 19, no. 4, pp. 1216–1225, Aug. 2014.

[2] L. Shang, S. Wang, M. Tan, and L. Cheng, "Swimming locomotion modeling for biomimetic underwater vehicle with two undulating long-fins," *Robotica*, vol. 30, no. 6, pp. 913–923, 2012.

[3] Q. Wei, S. Wang, Y. Wang, and M. Tan, "Course and depth control for a biomimetic underwater Vehicle-RobCutt-I," *Int. J. Offshore Polar Eng.*, vol. 25, no. 2, pp. 81–87, 2015.

[4] L. Wen, T. Wang, G. Wu, and J. Liang, "Quantitative thrust efficiency of a self-propulsive robotic fish: Experimental method and hydrodynamic investigation," *IEEE/ASME Trans. Mechatron.*, vol. 18, no. 3, pp. 1027–1038, Jun. 2013.

[5] S. Jin, J. Kim, J. Kim, and T. Seo, "Six-degree-of-freedom hovering control of an underwater robotic platform with four tilting thrusters via selective switching control," *IEEE/ASME Trans. Mechatron.*, vol. 20, no. 5, pp. 2370–2378, Oct. 2015.

[6] G. Antonelli, F. Caccavale, and S. Chiaverini, "Adaptive tracking control of underwater vehicle-manipulator systems based on the virtual decomposition approach," *IEEE Trans. Robot.*, vol. 20, no. 3, pp. 594–602, Jun. 2004.

[7] D. R. Yoerger, J. G. Cooke, and J. J. E. Slotine, "The influence of thruster dynamics on underwater vehicle behavior and their incorporation into control system design," *IEEE J. Ocean. Eng.*, vol. 15, no. 3, pp. 167–178, Jul. 1990.

[8] J. J. Fernandez, M. Prats, P. J. Sanz, J. C. Garcia, R. Marin, M. Robinson, D. Ribas, and P. Ridao, "Grasping for the seabed: Developing a new underwater robot arm for shallow-water intervention," *IEEE Robot. Autom. Mag.*, vol. 20, no. 4, pp. 121–130, Dec. 2013.

[9] G. Antonelli, "Underwater robots: Kinematic control of UVMSs," in Springer Tracts Advanced Robotics. Heidelberg, Germany: Springer-Verlag, 2014.

[10] T. J. Tarn, G. A. Shoults, and S. P. Yang, "A dynamic model of an underwater vehicle with a robotic manipulator using Kanes method," *Auton. Robot.*, vol. 3, no. 2, pp. 271–285, 1996.

[11] O. Korkmaz, S. K. Ider, and M. K. Ozgoren, "Control of an underactuated underwater vehicle manipulator system in the presence of parametric uncertainty and disturbance," in *Proc. 2013 Amer. Contr. Conf.*, Washington, DC, USA, 2013, pp. 578–584.

[12] J. Han, J. Park, and W. K. Chung, "Robust coordinated motion control of an underwater vehicle-manipulator system with minimizing restoring moments," *Ocean. Eng.*, vol. 38, no. 10, pp. 1197–1206, 2011.

[13] J. Han and W. K. Chung, "Active use of restoring moments for motion control of an underwater vehicle-manipulator system," *IEEE J. Ocean. Eng.*, vol. 39, no. 1, pp. 100–109, Jan. 2014.

[14] M. Santhakumar, "Investigation into the dynamics and control of an underwater vehicle-manipulator system," *Model. Simul. Eng.*, vol. 2013, no. 17, pp. 1–14, 2013.

[15] B. Lynch and A. Ellery, "Efficient control of an AUV-manipulator system: An application for the exploration of Europa," *IEEE J. Ocean. Eng.*, vol. 39, no. 3, pp. 552–570, Jul. 2014.

[16] N. Sarkar and T. K. Podder, "Coordinated motion planning and control of autonomous underwater vehicle-manipulator systems subject to drag optimization," *IEEE J. Ocean. Eng.*, vol. 26, no. 2, pp. 228–239, Apr. 2001.

[17] S. Mohan and J. Kim, "Indirect adaptive control of an autonomous underwater vehicle-manipulator system for underwater manipulation tasks," *Ocean. Eng.*, vol. 54, no. 22, pp. 233–243, 2012.

[18] M. Santhakumar, "Task space trajectory tracking control of an underwater vehicle-manipulator system under ocean currents," *Indian J. Geo-Marine. Sci.*, vol. 42, no. 6, pp. 675–683, 2013.

[19] G. Antonelli and S. Chiaverini, "Fuzzy redundancy resolution and motion coordination for underwater vehicle-manipulator systems," *IEEE Trans. Fuzzy Syst.*, vol. 11, no. 1, pp. 109–120, Feb. 2003.

[20] G. Antonelli and S. Chiaverini, "A fuzzy approach to redundancy resolution for underwater vehicle-manipulator systems," *Contr. Eng. Pract.*, vol. 11, no. 4, pp. 445–452, 2003.

[21] C. H. Farias dos Santos and E. R. de Pieri, "Functional machine with Takagi–Sugeno inference to coordinated movement in underwater vehicle-manipulator systems," *IEEE Trans. Fuzzy Syst.*, vol. 21, no. 6, pp. 1105–1114, Dec. 2013.
[22] B. Xu, S. R. Pandian, N. Sakagami, and F. Petry, "Neuro-fuzzy control of underwater vehicle-manipulator systems," *J. Franklin Inst.*, vol. 349, no. 3, pp. 1125–1138, 2012.
[23] E. Olguin-Diaz, G. Arechavaleta, G. Jarquin, and V. Parra-Vega, "A passivity-based model-free force-motion control of underwater vehicle-manipulator systems," *IEEE Trans. Robot.*, vol. 29, no. 6, pp. 1469–1484, Dec. 2013.
[24] Z. H. Ismail and M. H. Dunnigan, "Tracking control scheme for an underwater vehicle-manipulator system with single and multiple sub-regions and sub-task objectives," *IET Contr. Theory Appl.*, vol. 5, no. 5, pp. 721–735, 2011.
[25] N. Sakagami, M. Shibata, S. Kawamura, T. Inoue, H. Onishi, and S. Murakami, "An attitude control system for underwater vehicle-manipulator systems," in *Proc. IEEE Int. Conf. Robot. Autom.*, Anchorage, AK, USA, 2010, pp. 761–1767.
[26] G. Marani, S. K. Choi, and J. Yuh, "Underwater autonomous manipulation for intervention missions AUVs," *Ocean. Eng.*, vol. 36, no. 1, pp. 15–23, 2009.
[27] T. W. Kim and J. Yuh, "Development of a real-time control architecture for a semi-autonomous underwater vehicle for intervention missions," *Contr. Eng. Pract.*, vol. 12, no. 12, pp. 1521–1530, 2004.
[28] M. Prats, D. Ribas, N. Palomeras, J. C. García, V. Nannen, S. Wirth, J. J. Fernández, J. P. Beltrán, R. Campos, P. Ridao, P. J. Sanz, G. Oliver, M. Carreras, N. Gracias, R. Marłn, and A. Ortiz, "Reconfigurable AUV for intervention missions: A case study on underwater object recovery," *Intell. Service Robot.*, vol. 5, no. 1, pp. 19–31, 2012.
[29] D. Ribas, N. Palomeras, P. Ridao, M. Carreras, and A. Mallios, "Girona 500 AUV: From survey to intervention," *IEEE/ASME Trans. Mechatron.*, vol. 17, no. 1, pp. 46–53, Feb. 2012.
[30] E. Simetti, G. Casalino, S. Torelli, A. Sperinde, and A. Turetta, "Floating underwater manipulation: Developed control methodology and experimental validation within the TRIDENT project," *J. Field Robot.*, vol. 31, no. 3, pp. 364–385, 2014.
[31] D. Ribas, P. Ridao, A. Turetta, C. Melchiorri, G. Palli, J. J. Fernandez, P. J. Sanz, "I-AUV mechatronics integration for the TRIDENT FP7 project," *IEEE/ASME Trans. Mechatron.*, vol. 20, no. 5, pp. 2583–2592, Oct. 2015.
[32] O. Kermorgant, Y. Petillot, and M. Dunnigan, "A global control scheme for free-floating vehicle-manipulators," in *Proc. IEEE/RSJ Int. Conf. Intell. Robots Syst.*, Tokyo, Japan, 2013, pp. 5015–5020.
[33] J. R. Bemfica, C. Melchiorri, L. Moriello, G. Palli, and U. Scarcia, "A three-fingered cable-driven gripper for underwater applications," in *Proc. IEEE Int. Conf. Robot. Autom.*, Hong Kong, China, 2014, pp. 2469–2474.
[34] W. Zhang, H. Xu, and X. Ding, "Design and dynamic analysis of an underwater manipulator," in *Intelligent Technology and Systems*. New York, NY, USA: Springer-Verlag, 2015, pp. 399–409.
[35] C. Barbalata, M. W. Dunnigan, and Y. Petillot, "Dynamic coupling and control issues for a lightweight underwater vehicle manipulator system," in *Proc. IEEE Oceans*, St. John's, NL, USA, 2014, pp. 1–6.
[36] Z. Cai, *Robotics*. Beijing, China: Tsinghua Univ. Press, 2000.
[37] H. Li, Y. L. Chen, T. Chang, X. Wu, Y. Ou, and Y. Xu, "Binocular vision positioning for robot grasping," in *Proc. IEEE Int. Conf. Robot. Biomimetics*, Phuket, Thailand, 2011, pp. 1522–1527.

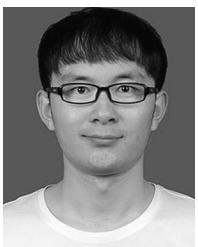

Yu Wang received the B.S. degree in automation from the Beijing Institute of Technology, Beijing, China, in July 2011. He is currently working toward the Ph.D. degree in control theory and control engineering at the State Key Laboratory of Management and Control for Complex Systems, Institute of Automation, Chinese Academy of Sciences, Beijing.

His research interests include intelligent control, robotics, and biomimetic robots.

Shuo Wang received the B.E. degree in electrical engineering from the Shenyang Architecture and Civil Engineering Institute, Shenyang, China, in 1995, the M.E. degree in industrial automation from the Northeastern University, Shenyang, in 1998, and the Ph.D. degree in control theory and control engineering from the Institute of Automation, Chinese Academy of Sciences, Beijing, China, in 2001.

He is currently a Professor in the State Key Laboratory of Management and Control for Complex Systems, Institute of Automation, Chinese Academy of Sciences. His research interests include biomimetic robot, underwater robot, and multirobot systems.

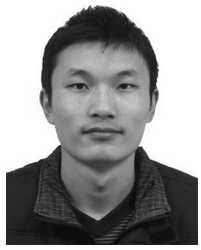

Qingping Wei received the B.S. degree in automation from University of Electronic Science and Technology of China, Chengdu, China, in July 2010, and the Ph.D. degree in control theory and control engineering from the State Key Laboratory of Management and Control for Complex Systems, Institute of Automation, Chinese Academy of Sciences, Beijing, China, in July 2015.

He is currently a Researcher at Dongfang Electric Corporation. His research interests include intelligent control and robotics.

Min Tan received the B.E. degree from Tsinghua University, Beijing, China, and the Ph.D. degree in control theory and control engineering from the Institute of Automation, Chinese Academy of Sciences, Beijing, in 1986 and 1990, respectively.

He is currently a Professor in the State Key Laboratory of Management and Control for Complex Systems, Institute of Automation, Chinese Academy of Sciences. His research interests include advanced robot control, biomimetic robot, multirobot system.

Chao Zhou received the B.S. degree (Hons.) in automation from Southeast University, Nanjing, China, in July 2003, and the Ph.D. degree in control theory and control engineering from the Institute of Automation, Chinese Academy of Sciences, Beijing, China, in 2008.

From July 2008, he was an Assistant Professor in the Key Laboratory of Complex Systems and Intelligent Science, Institute of Automation, Chinese Academy of Sciences, where he has been an Associate Professor since October 2011. His current research interests include the motion control of robot, the bio-inspired robotic fish, and embedded system of robot.

Junzhi Yu (SM'14) received the B.E. degree in safety engineering and the M.E. degree in precision instruments and mechanology from the North China Institute of Technology, Taiyuan, China, in 1998 and 2001, respectively, and the Ph.D. degree in control theory and control engineering from the Institute of Automation, Chinese Academy of Sciences (IACAS), Beijing, China, in 2003.

He is currently a Professor with the State Key Laboratory of Management and Control for Complex Systems, IACAS. His research interests include biomimetic robots, intelligent control, and intelligent mechatonic systems.

Dr. Yu is the Associate Editor of the IEEE TRANSACTIONS ON ROBOTICS and *Journal of Mechanical Science and Technology*, and as the Technical Editor of the IEEE/ASME TRANSACTIONS ON MECHATRONICS.